Received June 5, 2020, accepted June 30, 2020, date of publication July 13, 2020, date of current version July 23, 2020.

Digital Object Identifier 10.1109/ACCESS.2020.3009057

Full Band Compact Power Arm Subsystem With High Directive Sample

MAHMOUD ELSAADANY[1], (Member, IEEE), SHOUKRY I. SHAMS[1], (Member, IEEE), MOHAMED MAMDOUH M. ALI[1,2], (Graduate Student Member, IEEE), ABDEL-RAZIK SEBAK[1], (Life Fellow, IEEE), AND WALAA HAMOUDA[1], (Senior Member, IEEE)

[1]Department of Electrical and Computer Engineering, Concordia University, Montréal, QC H3G 1M8, Canada
[2]Department of Electrical Engineering, Assiut University, Assiut 71543, Egypt

Corresponding author: Mohamed Mamdouh M. Ali (mohamed.ali@ieee.org)

ABSTRACT An output arm is the first subsystem in the microwave components chain connected immediately after the power amplifier. These arms are responsible for transferring the signal from the output port of the power amplifier to the standard line of the system. The second objective is to obtain directive samples for both forward and backward signals. The typical design process for such a subsystem is carried out through the design of separate components, independently. This limits the achievable performance of the entire system and introduces excessive losses at intermediate flanges. In this work, we present a novel approach to design such a subsystem using a global optimization procedure. Specifically, we address both compactness and full-band operation of output arms deployed in radar applications. Analysis and design of each component in the proposed subsystem are illustrated. The presented subsystem achieves a deep matching level of 19 dB within an overall length below $2\lambda_g$. Moreover, the directive sample obtained through the presented design has an ultra-flat response of 20 dB $\pm$ 0.5 dB over the entire band of operation, while the directivity of the samples exceeds 18 dB. The measured results of the fabricated prototype have an excellent agreement with the simulations.

INDEX TERMS Full-band, high-power, power arm, waveguide standard.

I. INTRODUCTION

A mong all microwave subsystems, the output arms have significant importance. These arms are connected directly to the power source to provide a standard interface [1], [2]. In addition, these arms are responsible for collecting directive samples of both the forward and backward signals. Traditional implementation of these subsystems involves the use of an adapter cascaded with a dual directional coupler [3]–[5]. Other implementations include isolators to protect the source, however, we will focus our discussion on the common configuration of the reciprocal-type output arms. The major specifications of output arms are the deep matching provided by the adapter, the flat coupling, and the high directivity extracted through the coupler [6], [7]. These major characteristics have to be satisfied over the full band of operation. In the literature, this topic is frequently visited on the component level, where the adapters and directional couplers are discussed separately.

A variety of adapter designs exist in the literature that provide deep matching levels transitioning from coaxial line to traditional guiding structures; such as rectangular waveguide [8], [9], or the modern guiding structures; such as ridge gap waveguides and substrate integrated waveguides [10]–[13]. Most of the aforementioned work focuses either on the deep matching level or on the wide operating bandwidth, which leaves a room for improved designs. There are two basic configurations for the coaxial to waveguide transitions, the right angle and the end-launch [14]–[18]. The end-launch type is more convenient for the system installation as it ensures the alignment between the power source and the rest of the system. However, this configuration is more difficult in achieving the electrical specifications in terms of the matching level and the wide operating bandwidth.

On the other hand, the directional couplers have gone through a great development process over the past six decades. Directional couplers are one of the most famous Bi-conjugate networks [19]. Many configurations have been deployed to provide different coupling mechanisms. The broad-wall directional couplers, the 3-dB hybrid couplers, and the side wall couplers are examples of different types of

The associate editor coordinating the review of this manuscript and approving it for publication was Yanbo Chen.

couplers [20]–[23]. In addition, the implementation methodology of various types of couplers has been well investigated in the literature. Multiple printed guiding structures have been proposed for coupler implementations such as microstrip lines, substrate integrated waveguides, and printed ridge gap waveguide [24]–[28]. Among all configurations, loop couplers have the cutting edge in terms of the compactness [29]. They can be considered as one of the most compact types of directional couplers, where the challenge is usually in achieving a flat coupling response and sufficient directivity over a wide bandwidth.

In this work, we present a complete subsystem incorporating both an end-launch adapter and a loop coupler in one unit. With this configuration, we eliminate inter-flange reflections and provide optimized overall performance. The challenges associated with the design of end-launch adapter and the waveguide loop coupler are addressed, where the overall subsystem shows attractive performance. Therefore, the main contributions in this paper can be summarized as follows.

- A full band end launch adapter with a deep matching of 19 dB is proposed.
- A full band compact waveguide loop coupler with a flat coupling of 20 dB $\pm$ 0.5 and high directivity more than 18 dB is presented.
- An overall optimized design of a compact power arm subsystem with superior characteristics is proposed.

This paper is organized as follows: Section II lists the general specifications required for the output arm. Section III provides a detailed discussion about the end-launch adapter design procedure. This is followed by the analysis and the design of the loop coupler in Section IV. Section V presents the global optimization process for the proposed power arm subsystem.In Section VI, the fabrication considerations, and the measured results are illustrated. performance evaluation of the proposed subsystem components is presented in Section VII. Finally, the paper outcomes are summarized in Section VIII.

II. OUTPUT ARM SPECIFICATIONS

The design objective of this work is to provide an output arm for radar applications working in the extended S-band. The proposed design interfaces a coaxial power amplifier with an SC connector to a WR-229 rectangular waveguide standard system. The Standard threaded C coaxial connector (SC) is selected based on its superior power handling capability compared to both N-type and Threaded Neill–Concelman (TNC) connectors. The average power that can be handled by this type of connectors exceeds 1000 watt as indicated by many connector vendors, while N-type can handle less than half of this value. The output arm covers full band for WR229 standard, from 3.3 GHz to 4.9 GHz. The output arm will provide two different coupling values 40 dB and 60 dB with directivity exceeds 18 dB for both cases. Two different levels of coupling are supported to enable handling different power levels at the input port.

III. END LAUNCH ADAPTER DESIGN

Typically adapters are used to transfer the signal from one guiding structure to another. Here, the end-launch coaxial adapter converts the Transverse Electromagnetic (TEM) mode carried by the coaxial connector to Transverse Eclectic (TE) mode inside a standard waveguide. The design of this transition can be divided into two parts. The first part is a mode conversion section, where the signal propagating mode is converted from a TEM mode inside the coaxial to a TE mode inside a single ridge section. This is followed by a single ridge to a rectangular waveguide multi-section transformer.

A. MODE CONVERTER SECTION

The mode converter section is responsible only to change the TEM mode into a TE mode propagates inside a single ridge section. The inner conductor of the coaxial line is directly connected to the ridge. The Teflon filling of the coaxial line is extended to set on the same ridge. This technique is deployed to enable the maximum power handling capability of the structure. The alternative solution includes having an air-filled coaxial line, which will have a relatively small outer diameter to keep the characteristics impedance at the same value. The single ridge section is designed to have a 50Ω impedance with a cut underneath the ridge deployed as a tuning element. The ridge width and gap height are 0.582 inch and 0.174 inch, respectively. The groove underneath the single ridge has a height of $h_c = 0.457$ and depth of $d_c = 0.308$ as indicated in Fig. 1. Moreover, the response of the mode converter section is illustrated in Fig. 1(c), which shows a matching level beyond 15 dB for the mode converter alone. It worth mentioning that this will pass through a global optimization process with the second stage and the waveguide loop coupler to obtain a better matching level for the whole power arm.

B. SINGLE RIDGE TO RECTANGULAR WAVEGUIDE TRANSFORMER

This section is responsible for transforming the signal from the single ridge with 50Ω impedance to the rectangular waveguide. The design of this matching transformer starts with the analysis of the single ridge waveguide. This structure has been analyzed by Cohn [30], who introduced expressions for the cutoff frequency and the characteristic impedance. The single ridge structure is defined by four parameters, the guide width, the guide height, the ridge width and the gap height above the ridge, which will be denoted by A, B, C and D, respectively, the following phases will be defined:

$$\theta_1 = 2\pi \frac{(A-C)/2}{\lambda_c'} \quad \theta_2 = 2\pi \frac{C/2}{\lambda_c'} \tag{1}$$

where λ_c' represents the cutoff wavelength of the single ridge structure. This cutoff wavelength can be related to the cut off wavelength of the guide without ridge λ_c as follow:

$$\lambda_c' = \left(\frac{\pi/2}{\theta_1 + \theta_2}\right)\lambda_c \tag{2}$$

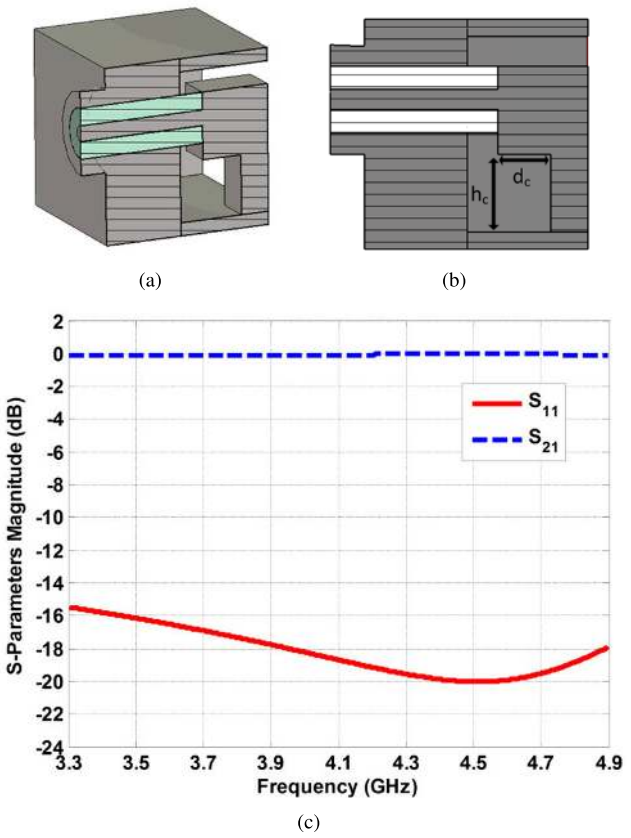

FIGURE 1. The mode converter section structure and response. (a) 3D cross-section view. (b) Side cross-section view. (c) Scattering parameters.

The above expressions are obtained through dividing the ridge into three parallel admittance sections (an open circuited line, a short circuited line, and the discontinuity B_0). This can be expressed as follows:

$$\frac{D}{B} = \frac{\cot(\theta_1) - B_0/Y_{01}}{\tan(\theta_2)} \tag{3}$$

where Y_{01} represents the single ridge characteristic admittance of the dominant mode. The term B_0/Y_{01} has been represented by very accurate empirical expressions by Whinery and Jamieson in [31]. To design the matching transformer, the characteristic impedance of the single ridge structure will be defined at infinite frequency $Z_{0,\infty}$ as the ratio between the voltage to the total current at the center of the guide, which can be given as:

$$Z_{0,\infty} = \frac{DE_0}{2\int_0^{C/2} i\, dl} = \frac{120\pi D}{\lambda_c\left(\sin(\theta_2) + \frac{D}{B}\cos(\theta_2)\tan(\theta_1/2)\right)} \tag{4}$$

while the guide impedance at any frequency is related to the guide impedance at ∞ with the following expression:

$$Z_0 = Z_{0,\infty}\frac{1}{\sqrt{1-(\lambda/\lambda_c')^2}} \tag{5}$$

The objective is to build a matching transformer to match between the single ridge structure at the mode converter section and the rectangular waveguide section.

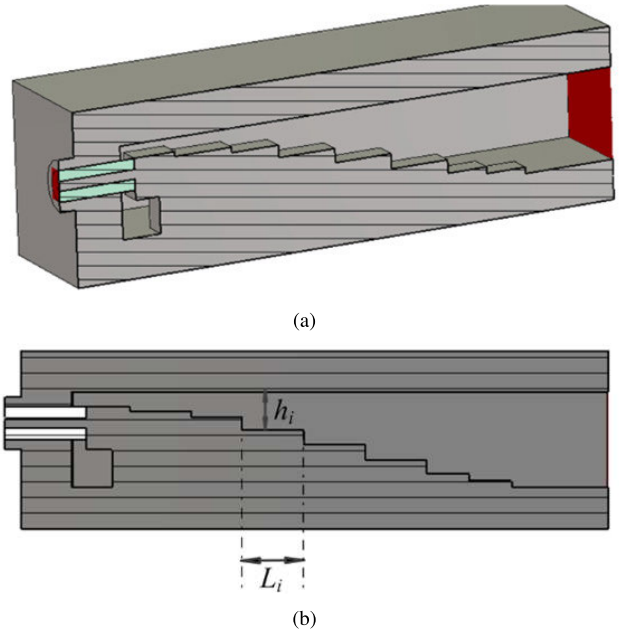

FIGURE 2. The end-launch adapter structure and response. (a) 3D cross-section view. (b) Side cross-section view.

The impedance of the rectangular waveguide section is calculated using the V^2/P definition [32]. A Chebyshev seven-sections matching transformer is designed, where the initial dimensions are obtained analytically. Hence a global optimization process is performed to obtain a matching level beyond 22 dB for the end launch adapter. Any impedance is calculated exactly at the center frequency, while all ridges are designed to have the same width 0.582 inch. In addition, all single ridge sections have the same guide width and height, $W_g = 2.29$ inch and $H_g = 1.145$ inch. These values are exactly equal to the opening of the standard WR-229 rectangular waveguide. As a result, each section has two major parameters deployed in the global optimization process, which are the gap height above the ridge h_i and the section length L_i.

IV. COMPACT WAVEGUIDE LOOP COUPLER DESIGN

In this section, we present a mathematical formulation for the required waveguide loop coupler shown in Fig. 3(a), where there are two secondary arms connected to the main arm to form a dual loop coupler. The main purpose from using two secondary arms is to provide a forward coupling (60 dB) and a reverse coupling (40 dB) as the forward signal power level is always much higher than the reverse one. Loop coupler is considered among the weak coupling structures, where it consists of two dissimilar guiding structure (waveguide and coaxial line) coupled through a coupling hole [5], [33], [34]. The primary arm, which is carrying most of the signal power is entitled the main arm. On the other hand, the secondary arm carries a small sample of the signal.

The suggested device is designed over two steps. The first step is obtaining the initial dimensions for the proposed design that satisfy the required coupling values. The second step is to tune the critical dimensions through the global optimization process to achieve a flat coupling and the

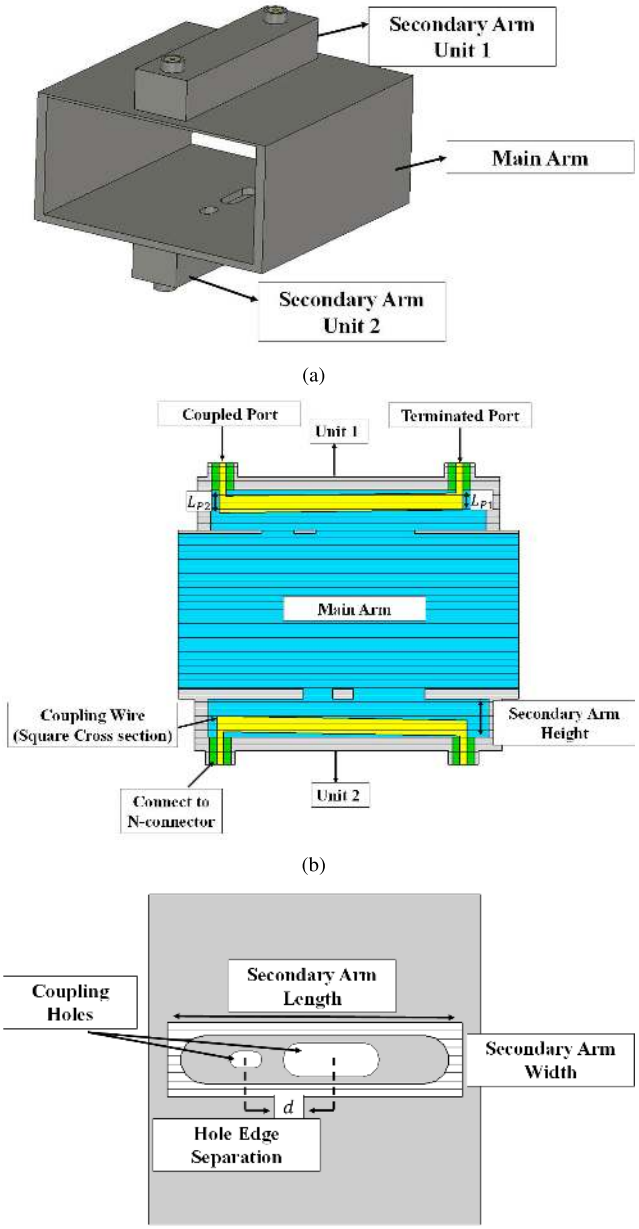

FIGURE 3. (a) 3-D view of dual loop coupler. (b) Side view cross-sectional. (c) Top view cross-sectional.

required directivity when it connected with the end launch adapter forming the power arm . The main arm is a WR-229 rectangular waveguide operating in the required operating frequency band. The secondary arm consists of a cavity that contains two coaxial ports with inner conductors connected through the coupling wire. The dimensions of the second arm are selected in order to match a 50 Ohm N-connector.

The analysis of loop coupler design was visited in many previous publications, where a single circular or rectangular hole is deployed to provide the required coupling value [35]–[37]. In this work, two rectangular holes with a separation distance d are placed to add more degrees of freedom in the design parameters as shown in Fig. 3(c). Assuming the length and the width of the rectangular hole

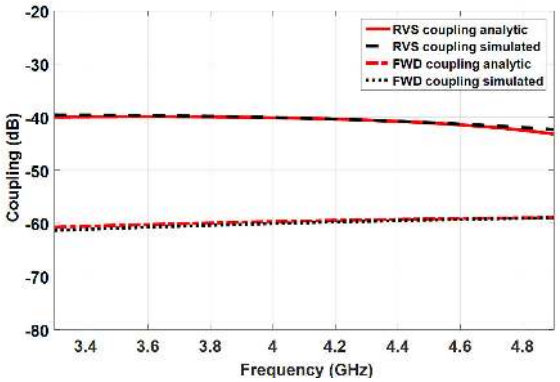

FIGURE 4. Comparison between the simulated and analytic 40 dB coupling.

are L_{hi} and W_{hi} $(i = 0, 1, 2, \ldots N)$, the coupling C_i of ith hole are related the hole dimensions as:

$$C_i = H_f L_{hi}^2 W_{hi}^4 \tag{6}$$

where, H_f is constant for the coupling coefficient which can be written in simple form as:

$$H_f = \left[\frac{\pi}{32} k_o \sqrt{\frac{2}{ab}} \sqrt{\frac{\lambda}{\lambda_g}} \sqrt{\frac{1}{(F(k)}} (\frac{4}{3} A_m + \frac{\lambda_g}{\lambda} A_e)\right]^2 \tag{7}$$

where, $k_o = \frac{\omega}{c}$ is the free space wave number, $a \times b$ is the cross section dimension of the main arm, λ is the free space wavelength, λ_g is the guided wavelength in the main arm, and $F(k)$ is a constant which is related to the secondary arm parameters, which can be found in [35]–[37]. Also, A_e and A_m represent the wall thickness correction factors which correct both the electric and magnetic polarizabilites that are given in [38], [39].

Based on the analysis of multi-hole dissimilar coupler that were addressed before in the literature, the coupling of N holes can be expressed as [40]–[42]:

$$C = \sum_{i=0}^{N} H_f L_{hi}^2 W_{hi}^4 e^{-2j\theta i} \tag{8}$$

where, $\theta = \frac{\theta_s + \theta_p}{2}$, $\theta_p = \beta d$, and $\theta_s = k_o d$, while β is the phase constant in the main arm.

The initial values for the coupling hole dimensions, holes spacing, and wall thickness are selected to satisfy the coupling values from the previous equation. Assuming that the coupling holes have the same length and width, the comparison between the simulated and analytic forward and reverse coupling over the operating frequency band is shown in Fig. 4. The proposed model can accurately estimate the coupling, which can accelerate the design process of the waveguide loop coupler.

Some modifications are added to the proposed design to give a degree of freedom through the global optimization process in adjusting the required directivity and coupling flatness over the operation frequency band which include:

- Rounding the coupling holes edges
- The inner pin of the N-connector having different lengths which result in a sloping for the coupling wire.

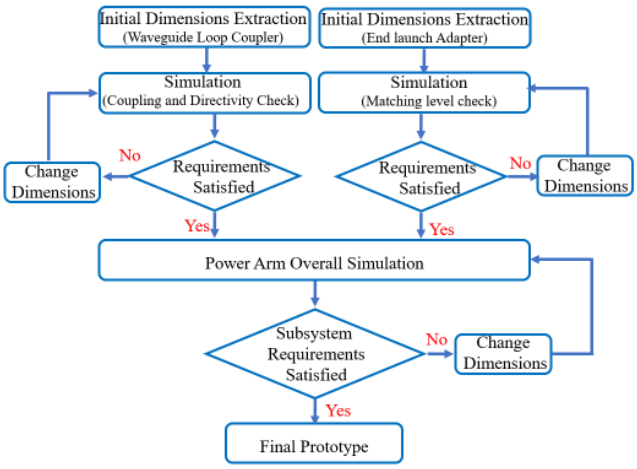

FIGURE 5. The proposed global optimization flowchart.

TABLE 1. The final dimensions of the matching network sections in millimeter.

Section i	h_i	L_i	Section i	h_i	L_i
1	0.232	0.739	5	0.817	0.739
2	0.299	0.609	6	0.984	0.515
3	0.453	0.739	7	1.066	0.516
4	0.628	0.800			

V. GLOBAL OPTIMIZATION

Global optimization is an operation of finding the overall best performance for the proposed power arm achieving a compact size. In the previous sections, We discussed the design procedures to extract the initial dimensions of the power arm components. However, the integration of the end launch adapter with the loop coupler having these initial dimensions still needs further optimization to achieve better overall performance. This is due to the loading effect of the coupler slots located in the middle of the main waveguide. In addition, the fabrication of both units in one body will eliminate the possible performance deterioration at the intermediate flanges. Therefore, global optimization is performed to achieve a compact size, deep matching level, and low losses over a full-band operation. A flowchart presenting the global optimization process is shown in Fig. 5. This optimization results in the optimum dimensions for both the adapter and the loop coupler that are listed in Tables 1 and 2, respectively. Table 1 shows the final dimensions for the gap height above the ridge h_i and the section length L_i for the end launch adapter. Regrading the loop coupler, the coupling wall thickness is $0.024''$ and $0.069''$ for Unit 1 and Unit 2, respectively. The coupling wires have a square cross-section $0.124'' \times 0.124''$ for Unit 1 and $0.115'' \times 0.115''$ for Unit 2. These wires are soldered to the inner pin of the N- connectors from both ends. The inner pin length measured from the base of the inserts at the coupled and the terminated ports L_{p1} and L_{p2}, respectively. These dimensions, as well as the wire length, are listed in Table 2, while the simulated return loss, coupling, and directivity will be compared with the measurement in the experimental validation section.

TABLE 2. Secondary arm optimized dimensions for both units.

Dimension		Value in inches	
		Unit 1 (40 dB)	Unit 2 (60 dB)
Secondary Arm	Length	2.02	2.06
	Width	0.36	0.28
	Height	0.294	0.283
Coupling holes	Length	0.24, 0.727	0.212, 0.524
	Width	0.126, 0.257	0.14, 0.175
	Edge separation	0.158	0.151
Coupling Wires	Length	1.74	1.78
	L_{P1}	0.144	0.125
	L_{P2}	0.167	0.175

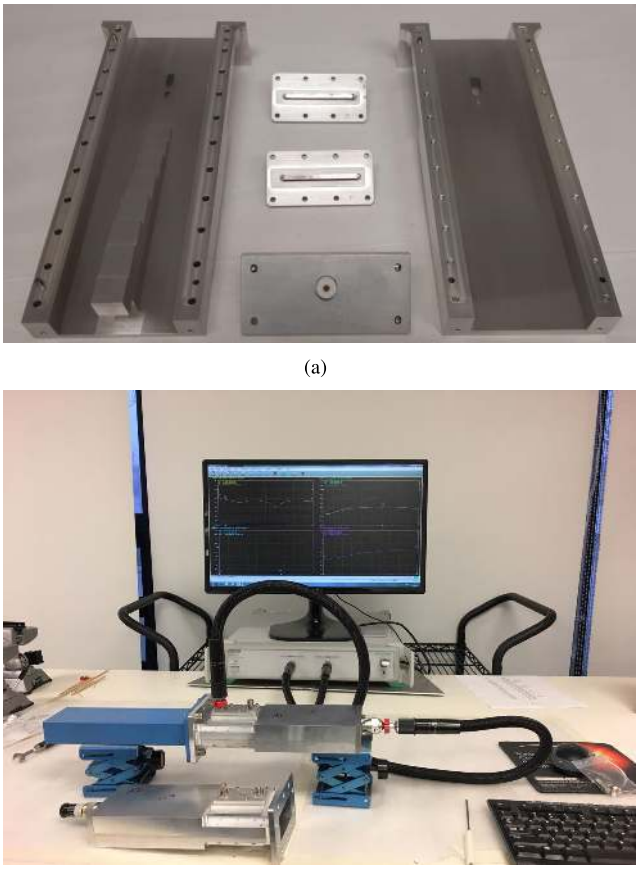

(a)

(b)

FIGURE 6. (a) Fabrication parts of the proposed design. (b) The measurement setup for the output arm subsystem.

VI. EXPERIMENTAL VALIDATION

The fabrication of all parts, shown in Fig.6(a), is performed on (MATSUURA MC-510VG) Computer Numerically Controlled (CNC) machine, which has a tolerance of $0.0005''$ in all dimensions. The proposed output arm is assembled and tested as shown in Fig. 6(b). The measurements were performed through ANRITSU MS4322 Vector Network Analyzer (VNA), where two measurement sets have been performed to evaluate both the adapter and the coupler performance in the proposed subsystem. The first set of measurements is carried out with a single port calibration at a standard WR-229 waveguide port. The deployed calibration methodology is the double offset short technique with an offset length of 12.78 mm. The coaxial connector side

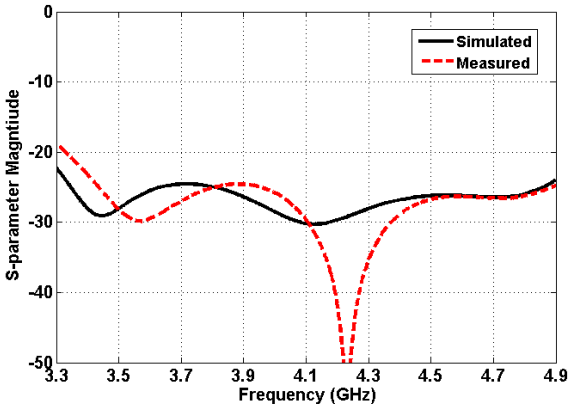

FIGURE 7. Comparison between the simulated and the measured return loss for the power arm.

is terminated with an SC precision termination, where the measured return loss is compared to simulated one in Fig.7. This figure shows an excellent agreement between both the measured and the simulated results. The simulated model assumes full matching at the coaxial connector, while the measured data replace this with a precision termination which has a slight effect on the measured result.

Afterward, the VNA is calibrated by ANRITSU TOSLKF50A-40, a Short-Open-Load-Through (SLOT) coaxial calibration kit with an SubMiniature version K (SMK) interface. The coupled port has an SubMiniature version A (SMA) interface, which inter-mat with the SMK interface. On the other hand, an SMA-SC converter is deployed to interface the main arm. Through this setup, both the coupling and the directivity are measured and compared with the simulated results in Fig. 8 (a) and (b). These figures show an excellent agreement in the coupling curves, however, the directivity has a tangible deviation. The assembly process of the loop coupler contains manual welding to connect the wire and the inner conductor of the coaxial connector. The manual process will result in an irregular shape, which has a slight impact on the coupling level as the coupling level and a significant effect on the directivity level. These figures, also, highlight the ultra-flat coupling level of both the forward and the reverse coupling responses. Moreover, the measured directivity exceeds 18 dB for both the forward and the reverse couplers over the entire operating bandwidth.

Although the coupled ports act as output ports only in the real system, the secondary arm return loss is measured and compared with the simulated model for a complete assessment of the proposed output arm. This comparison is shown in Fig. 9, where the forward coupling port has a better matching level in both the simulated and the measured curves. The measured secondary arm matching level of the forward coupler is below 20 dB at the lower end of the band, while it deteriorates to reach 12 dB at the higher end of the frequency band. The reverse coupler has a secondary arm matching level below 13 dB at the lower end and deteriorates to reach 7 dB at the higher end of the frequency band.

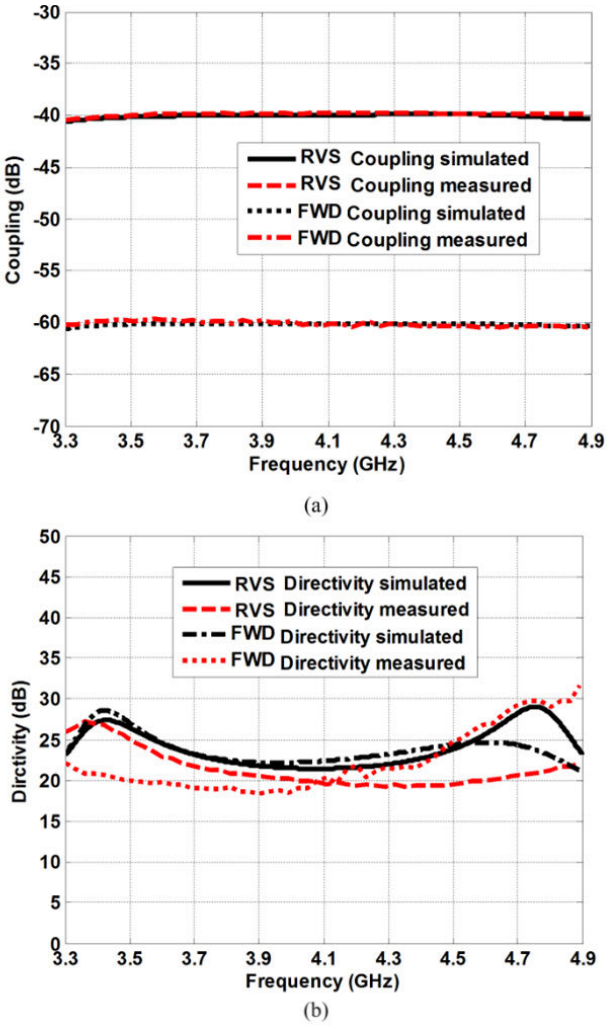

FIGURE 8. Comparison between the simulated and the measured return loss for both adapters.

VII. THE PROPOSED COMPONENTS PERFORMANCE EVALUATION

It is essential to highlight that one significant contribution of this work is to provide an overall optimized design of the entire subsystem. After calculating the initial dimensions of each component separately, the complete subsystem is optimized globally. This final optimization is carried out to elevate the overall system performance. The optimization goal is to enhance the matching level of the subsystem while keeping the coupling and the directivity within the designed range.

In this section, we present a comparison between the proposed design technique of the power arm components and the state of the art methods, which are summarized in Table. 3. The design of the end launch adapter is addressed intensively in many articles, where many types of adapters are proposed and analyzed. One type of end launch adapters is based on a coaxial loop within a rectangular waveguide [14]. This published work demonstrated a simple and low-cost fabrication process, however, a partial band with a low matching

TABLE 3. Comparison between end launch adapter and loop couplers designs.

End launch adapter				Loop coupler			
Ref.	Technique	RL	BW	Ref.	CPLG/DIR	RL	BW
[14]	Coaxial loop(SMA)	9.54 dB	33 %	[44]	± 0.5 dB/ 10 dB	15 dB	5 %
[4], [15]	H-plane Van (SMA)	15.5 dB	38 %	[45]	± 1 dB/ 20 dB	-0 dB	10 %
[16]	Taconic shape (SMA)	10 dB	44 %	[46]	± 1 dB/ 16 dB	20 dB	38 %
The proposed power ARM	(SC)	19 dB	44 %	-	± 0.5 dB/20 dB	19 dB	44 %

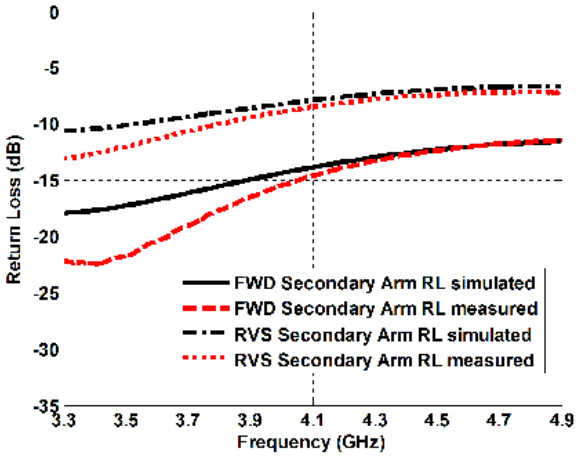

FIGURE 9. Comparison between the simulated and the measured return loss for both adapters.

level is achieved. Other techniques for end launch adapters is to use different probe shapes inserted into a rectangular H-plane vane in rectangular waveguide [4], [15]. Although a slight improvement for the matching level is achieved, this technique still has limited bandwidth. A full band end launch adapter based on using Taconic polygonal dielectric shape is presented in [16], however, a low matching level is achieved. Most of the above-mentioned articles used different techniques, which demonstrated either low matching level or narrow bandwidth. On the other hand, the proposed work is presented a design that can cover a full band operation with a deep matching level.

Regarding the waveguide loop coupler, many designs have been visited in the literature based on different coupling mechanisms. One traditional configuration based on a direct coupling between a wire and the waveguide is introduced in [43], which has relatively compact and very flat coupling (CPLG), however, it covers only 5 % bandwidth. Another configuration that has better bandwidth is depending on using a coupling conductor with protuberances [44]. Although this technique has improved the directivity (DIR) of the loop coupler, it degraded the coupling flatness. More bandwidth enhancement is achieved by using a straight line inside a cavity, where the coupling is achieved through a rectangular hole [45]. This configuration improved the bandwidth, however, a large coupling deviation with low directivity is achieved. On the other hand, the proposed coupler is adopted several modifications to achieve a full bandwidth of operation with flat coupling and high directivity compared with other published work. The deployed coupling holes in the proposed design consists of two successive holes, where the width and the length of both holes are used to control the coupling flatness and the directivity. In addition, the wire is designed with a slope to increase the directivity. Finally, the holes and the secondary arm cavity are designed with rounded ends to enhance the directivity.

VIII. CONCLUSION

A compact design for full band power arm subsystem with high directive sample has been introduced. The proposed subsystem consisting of both an end-launch adapter and waveguide loop coupler integrated into one unit with an overall length below $2\lambda_g$. The analysis and design of each component have been discussed, where initial dimensions of each component can be estimated. The presented design has achieved matching better than -20 dB. Moreover, the proposed design has a flat response with a samples directivity more than 18 dB over the entire operating frequency band. The proposed subsystem is fabricated and measured, where a good agreement between the simulated and measured results are achieved.

REFERENCES

[1] L. Schachter and J. A. Nation, "On the coupling between a quasiperiodic structure and an asymmetric output arm," *IEEE Trans. Microw. Theory Techn.*, vol. 43, no. 1, pp. 42–47, Jan. 1995.

[2] M. Elsaadany, A. Ali, and W. Hamouda, "Cellular LTE—A technologies for the future Internet-of-Things: Physical layer features and challenges," *IEEE Commun. Surveys Tuts.*, vol. 19, no. 4, pp. 2544–2572, 4th Quart., 2017, doi: 10.1109/COMST.2017.2728013.

[3] T. Djeddi, M. Elsaadany, S. Shams, and W. Hamouda, "Compact ultra-wideband printed bandpass filter based on coupled-line resonator loading," in *Proc. 18th Int. Symp. Antenna Technol. Appl. Electromagn. (ANTEM)*, Waterloo, ON, Canada, Aug. 2018, pp. 1–2, doi: 10.1109/ANTEM.2018.8572885.

[4] K. H. Kloke, "End-launched coaxial and microstrip to partial H-plane waveguide adapters," Ph.D. dissertation, Dept. Elect., Electron., Comput. Eng., Univ. Pretoria, Pretoria, South Africa, 2014.

[5] B. Maher, "An L-band loop-type coupler (correspondence)," *IEEE Trans. Microw. Theory Techn.*, vol. MTT-9, no. 4, pp. 362–363, Jul. 1961.

[6] E. Hassan, D. Noreland, E. Wadbro, and M. Berggren, "Topology optimisation of wideband coaxial-to-waveguide transitions," *Sci. Rep.*, vol. 7, no. 1, p. 45110, Apr. 2017.

[7] Y. Zhang, Q. Wang, and J. Ding, "A cross-guide waveguide directional coupler with high directivity and broad bandwidth," *IEEE Microw. Wireless Compon. Lett.*, vol. 23, no. 11, pp. 581–583, Nov. 2013, doi: 10.1109/LMWC.2013.2281407.

[8] M. E. Bialkowski, "Analysis of a coaxial-to-waveguide adaptor including a discended probe and a tuning post," *IEEE Trans. Microw. Theory Techn.*, vol. 43, no. 2, pp. 344–349, Feb. 1995.

[9] N. Rui-Xing, L. En, G. Gao-Feng, and W. Yi, "Simulation and design of 18–40 GHz ridge waveguide to coaxial transition," in *Proc. IEEE Int. Conf. Microw. Technol. Comput. Electromagn. (ICMTCE)*, May 2011, pp. 183–185.

[10] S. I. Shams and A. A. Kishk, "Wideband coaxial to ridge gap waveguide transition," *IEEE Trans. Microw. Theory Techn.*, vol. 64, no. 12, pp. 4117–4125, Dec. 2016.

[11] I. Afifi, M. M. M. Ali, and A.-R. Sebak, "Analysis and design of a wideband coaxial transition to metal and printed ridge gap waveguide," *IEEE Access*, vol. 6, pp. 70698–70706, 2018.
[12] A. A. Khan and M. K. Mandal, "A compact broadband direct coaxial line to SIW transition," *IEEE Microw. Wireless Compon. Lett.*, vol. 26, no. 11, pp. 894–896, Nov. 2016.
[13] S. Mukherjee, P. Chongder, K. V. Srivastava, and A. Biswas, "Design of a broadband coaxial to substrate integrated waveguide (SIW) transition," in *Proc. Asia–Pacific Microw. Conf. Proc. (APMC)*, Seoul, South Korea, Nov. 2013, pp. 896–898.
[14] D.-Y. Yang, "Design and fabrication of an end-launched rectangular waveguide adapter fed by a coaxial loop," *J. Inf. Commun. Converg. Eng.*, vol. 10, no. 2, pp. 103–107, Jun. 2012.
[15] K. H. Kloke, J. Joubert, and J. W. Odendaal, "Coaxial end-launched and microstrip to partial *H*-plane waveguide transitions," *IEEE Trans. Microw. Theory Techn.*, vol. 63, no. 10, pp. 3103–3108, Oct. 2015.
[16] N. Carmel, D. Elmakayes, and H. Matzner, "Investigation of a coax-to-waveguide transition element," in *Proc. IEEE Int. Conf. Microw., Commun., Antennas Electron. Syst. (COMCAS)*, Tel Aviv, Israel, Nov. 2011, pp. 1–3.
[17] H. Ma, B. Liang, Y. Shi, and J. Miao, "Analysis of coaxial-to-waveguide transitions in end launcher type," in *Proc. Int. Conf. Microw. Millim. Wave Technol. (ICMMT)*, Shenzhen, China, May 2012, pp. 1–4.
[18] K. K. Chan, R. Martin, and K. Chadwick, "A broadband end launched coaxial-to-waveguide transition for waveguide phased arrays," in *Proc. IEEE Antennas Propag. Soc. Int. Symp.*, Atlanta, GA, USA, Jun. 1998, pp. 1390–1393.
[19] L. J. Cutrona, "The theory of Bi-conjugate networks," *Proc. IRE*, vol. 39, no. 7, pp. 827–832, Jul. 1951.
[20] H. C. Early, "A wide-band directional coupler for wave guide," *Proc. IRE*, vol. 34, no. 11, pp. 883–886, Nov. 1946.
[21] M. D. Pozar, *Microwave Engineering*. Hoboken, NJ, USA: Wiley, 2005.
[22] R. E. Collin, *Foundations for Microwave Engineering*, 2nd ed. New York, NY, USA: McGraw-Hill, 1992.
[23] S. I. Shams and A. A. Kishk, "Design of 3-dB hybrid coupler based on RGW technology," *IEEE Trans. Microw. Theory Techn.*, vol. 65, no. 10, pp. 3849–3855, Oct. 2017.
[24] M. M. M. Ali and A.-R. Sebak, "2-D scanning magnetoelectric dipole antenna array fed by RGW butler matrix," *IEEE Trans. Antennas Propag.*, vol. 66, no. 11, pp. 6313–6321, Nov. 2018.
[25] M. M. M. Ali, S. I. Shams, and A.-R. Sebak, "Printed ridge gap waveguide 3-dB coupler: Analysis and design procedure," *IEEE Access*, vol. 6, pp. 8501–8509, 2018.
[26] R. C. Knechtli, "Further analysis of transmission line directional couplers," *Proc. IRE*, vol. 43, pp. 867–869, Jul. 1955.
[27] C.-H. Tseng, C.-H. Mou, C.-C. Lin, and C.-H. Chao, "Design of microwave dual-band rat-race couplers in printed-circuit board and GIPD technologies," *IEEE Trans. Compon., Packag., Manuf. Technol.*, vol. 6, no. 2, pp. 262–271, Feb. 2016.
[28] S. Kim, H. Aubert, and M. M. Tentzeris, "An inkjet-printed flexible broadband coupler in substrate integrated waveguide (SIW) technology for sensing, RFID and communication applications," in *IEEE MTT-S Int. Microw. Symp. Dig.*, Jun. 2014, pp. 1–4.
[29] S. I. Shams, M. Elsaadany, G. Saad, and A. A. Kishk, "Compact wideband dual loop coupler with high power handling capability for radar applications," *IEEE Microw. Wireless Compon. Lett.*, vol. 27, no. 10, pp. 900–902, Oct. 2017.
[30] S. B. Cohn, "Properties of ridge wave guide," *Proc. IRE*, vol. 35, no. 8, pp. 783–788, Aug. 1947.
[31] J. R. Whinnery and H. W. Jamieson, "Equivalent circuits for discontinuities in transmission lines," *Proc. IRE*, vol. 32, no. 2, pp. 98–114, Feb. 1944.
[32] G. I. Mattiaei, L. Young, and E. M. T. Jones, *Microwave Filters, Impedance-Matching Networks, and Coupling Structures*, 2nd. Norwood, MA, USA: Artech House, Nov. 1985.
[33] R. F. Schwartz, P. J. Kelly, and P. P. Lombardini, "Criteria for the design of loop-type directional couplers for the l band," *IEEE Trans. Microw. Theory Techn.*, vol. MTT-4, no. 4, pp. 234–239, Oct. 1956.
[34] J. Kulinski, E. Kur, and D. Bednarczyk, "Loop directional coupler for rectangular waveguides with small dimensions," in *Proc. 12th Int. Conf. Microw. Radar. Conf. (MIKON)*, Krakow, Poland, vol. 2, 1998, pp. 615–619.
[35] M. Kumar and B. N. Das, "Coupled transmission lines," *IEEE Trans. Microw. Theory Techn.*, vol. MTT-25, no. 1, pp. 7–10, Jan. 1977.
[36] W. Wang, M. Xu, G. Yu, G. LIU, and R. Shi, "The design of a waveguide-coaxial line directional coupler," *Int. J. Electron.*, vol. 74, no. 1, pp. 111–120, Jan. 1993.
[37] W. Wang, Y. Gong, J. Sun, and G. Yu, "Analysis and design of a waveguide-coaxial line single-hole directional coupler," *Int. J. Electron.*, vol. 81, no. 3, pp. 311–319, Sep. 1996.
[38] Y. Saito and D. S. Filipovic, "Analysis and design of monolithic rectangular coaxial lines for minimum coupling," *IEEE Trans. Microw. Theory Techn.*, vol. 55, no. 12, pp. 2521–2530, Dec. 2007.
[39] N. A. McDonald, "Electric and magnetic coupling through small apertures in shield walls of any thickness," *IEEE Trans. Microw. Theory Techn.*, vol. MTT-20, no. 10, pp. 689–695, Oct. 1972.
[40] M. M. M. Ali, S. I. Shams, and A.-R. Sebak, "Low loss and ultra flat rectangular waveguide harmonic coupler," *IEEE Access*, vol. 6, pp. 38736–38744, 2018.
[41] D. J. Lewis, "Mode couplers and multimode measurement techniques," *IEEE Trans. Microw. Theory Techn.*, vol. MTT-7, no. 1, pp. 110–116, Jan. 1959.
[42] M. M. M. Ali, S. I. Shams, A. Sebak, and A. A. Kishk, "Rectangular waveguide cross-guide couplers: Accurate model for full-band operation," *IEEE Microw. Wireless Compon. Lett.*, vol. 28, no. 7, pp. 561–563, Jul. 2018.
[43] M. Mazur and S. Kostka, "Loop coupler in rectangular waveguide working near to the cut-off frequency," in *Proc. 15th Int. Conf. Microw., Radar Wireless Commun.*, Warsaw, Poland, vol. 2, 2004, pp. 751–754.
[44] H. Ishibashi, M. Kurihara, Y. Tahara, H. Yukawa, T. Owada, and H. Miyashiya, "Waveguide loop-type directional coupler using a coupling conductor with protuberances," in *Proc. Eur. Microw. Conf. (EuMC)*, Paris, France, Sep. 2015, pp. 1026–1029.
[45] R. Karimian and M. D. Ardakani, "Ultra-compact C-band waveguide loop coupler for communication systems," *Int. J. Microw. Opt. Technol.*, vol. 10, no. 6, pp. 452–457, 2015.

MAHMOUD ELSAADANY (Member, IEEE) received the B.Sc. (Hons.) and M.Sc. degrees in electrical engineering from Cairo University, Egypt, in 2006 and 2010, respectively, and the Ph.D. degree in electrical and computer engineering from Concordia University, Montrŕal, QC, Canada, in 2018. He is currently a Research Professional with the École de technologie supérieure (ETS), Université du Québec. He was a Researcher with Qatar University, Qatar, from 2008 to 2010. His current research interests include digital signal processing, optimization of microwave components, machine-type communication, and algorithms design for the 5G cellular networks.

SHOUKRY I. SHAMS (Member, IEEE) received the B.Sc. (Hons.) and M.Sc. degrees in electronics and communications engineering from Cairo University, Egypt, in 2004 and 2009, respectively, and the Ph.D. degree in electrical and computer engineering from Concordia University, Montréal, QC, Canada, in 2016. From 2005 to 2006, he served as a Teaching and Research Assistant at the Department of Electronics and Communications Engineering, Cairo University. From 2006 to 2012, he served as a Teaching and Research Assistant with the IET Department, German University in Cairo. From 2012 to 2016, he was a Teaching and Research Assistant with Concordia University. He is currently an Affiliated Assistant Professor with the Department of Electrical and Computer Engineering, Concordia University. His research interests include microwave reciprocal/nonreciprocal design and analysis, high power microwave subsystems, antenna design, and material measurement. He received the Faculty Certificate of Honor, in 1999, the Distinction with Honor from Cairo University, in 2004, the Concordia University Recruitment Award, in 2012, and the Concordia University Accelerator Award, in 2016. He was the GUC-IEEE Student Branch Chair 2010-2012.

MOHAMED MAMDOUH M. ALI (Graduate Student Member, IEEE) received the B.Sc. (Hons.) and M.Sc. degrees in electronics and communications engineering from Assiut University, Egypt, in 2010 and 2013, respectively, and the Ph.D. degree in electrical and computer engineering from Concordia University, Montréal, QC, Canada, in 2020. From 2010 to 2015, he was a Teaching and Research Assistant with the Department of Electronics and Communications Engineering, Assiut University. He was a Teaching and Research Assistant with Concordia University, from 2016 to 2020. He is currently a Lecturer with the Department of Electrical Engineering, Faculty of Engineering, Assiut University. His current research interests include microwave reciprocal/nonreciprocal and antenna design.

ABDEL-RAZIK SEBAK (Life Fellow, IEEE) received the B.Sc. degree (Hons.) in electrical engineering from Cairo University, Cairo, Egypt, in 1976, the B.Sc. degree in applied mathematics from Ein Shams University, Cairo, in 1978, and the M.Eng. and Ph.D. degrees in electrical engineering from the University of Manitoba, Winnipeg, MB, Canada, in 1982 and 1984, respectively. From 1984 to 1986, he was with Canadian Marconi Company, involving in the design of microstrip phased array antennas. From 1987 to 2002, he was a Professor with the Department of Electronics and Communication Engineering, University of Manitoba. He is currently a Professor with the Department of Electrical and Computer Engineering, Concordia University, Montréal, QC, Canada. His research interests include phased array antennas, millimeter-wave antennas and imaging, computational electromagnetics, and interaction of EM waves with engineered materials and bio electromagnetics. He is a member of the Canadian National Committee of International Union of Radio Science Commission B. He was a recipient of the 2000 and 1992 University of Manitoba Merit Award for outstanding Teaching and Research, the 1994 Rh Award for Outstanding Contributions to Scholarship and Research, and the 1996 Faculty of Engineering Superior. He has served as the Chair for the IEEE Canada Awards and Recognition Committee from 2002 to 2004, as the Technical Program Chair for the 2002 IEEE CCECE Conference and the 2006 URSIANTEM Symposium, and was the Technical Program Co-Chair of the 2015 IEEE ICUWB Conference.

WALAA HAMOUDA (Senior Member, IEEE) received the B.Sc. degree in telecommunications and electronics from Ain Shams University, Cairo, Egypt, and the M.A.Sc. and Ph.D. degrees in electrical and computer engineering from Queen's University, Kingston, Canada, in 1998 and 2002, respectively. From 1994 to 1996, he worked as a System Engineer at Siemens Research and Development, Cairo. In July 2002, he joined the Department of Electrical and Computer Engineering, Concordia University, as an Assistant Professor, where he is currently a Full Professor. From September 2008 to May 2009, he was the Associate Chair of the Department of Electrical and Computer Engineering, Concordia University. His current research interests include wireless communications, cognitive radios, ad hoc networks, cross-layer design, MIMO communications, and power-line/smart-grid communications. During his Ph.D. study, he received many fellowships and scholarships, including the Ontario Graduate Scholarships (OGS), the Queen's Graduate Fellowship, the Queen's Graduate Award, the IEEE Student Conference Award (ICC2001), and the Outstanding-Engineering Award (Siemens).